Chapter 10

GaAsN Grown by Chemical Beam Epitaxy for Solar Cell Application

Kazuma Ikeda, Han Xiuxun, Bouzazi Boussairi and Yoshio Ohshita

Additional information is available at the end of the chapter

http://dx.doi.org/10.5772/51885

1. Introduction

InGaAsN is a candidate material to realize the ultrahigh efficiency lattice-matched multi-junction solar cell. This material has the 1eV band gap energy and same lattice constant as GaAs or Ge substrate by controlling the In and N compositions to be 9% and 3%, respectively [1, 2]. So far, the highest conversion efficiency of the lattice-matched multi-junction solar cell is 43.5% at 418-suns which was achieved by the 3-junction solar cell, GaInP/GaAs/GaInNAs [3]. By realizing the 4-junction device, InGaP/InGaAs/InGaAsN/Ge, the efficiency is expected to be 41% at 1-sun under the AM1.5G spectrum and 51% at 500-suns under the AM1.5D spectrum [4]. In order to achieve the expected super high efficiency, the short circuit current, J_{sc}, under a GaAs filter has to be 17 mA/cm^2 at 1-sun under AM0 conditions. However, the highest J_{sc} under that condition has been 10.9mA/cm^2. This corresponds to the 6.2% conversion efficiency and J_{sc}=26.0 mA/cm^2 without GaAs filters at 1-sun under AM1.5 [5]. The diffusion length of the minority carrier in this case is supposed to be much shorter than 1 μm which is required to achieve the ultrahigh efficiency. Therefore, the mobility and lifetime of the minority carrier should be improved.

The large miscibility gap is a particular characteristic of (In)GaAsN. It means that the phase separation easily occurs in the near equilibrium condition. It is caused by the large difference between the atomic radii of As and N [6]. Because of this property, homogeneous alloys are difficult to be obtained. Various growth techniques have been tried to avoid the phase separation and obtain good alloys: the plasma-assisted molecular beam epitaxy (MBE) [7], solid source MBE with a radio frequency (RF) nitrogen plasma source [8], metal organic vapor phase epitaxy (MOVPE) [9], metalorganic MBE [10-13], and chemical beam epitaxy (CBE) [14].

The chemical reactions at the surface of the substrates are expected to occur in the far-from-equilibrium states in those methods.

The electrical properties of (In)GaAsN has been reported to be drastically deteriorated by increasing the N composition [15]. The Hall hole mobility of p-GaAsN as a function of the N composition is shown in Figure 1 [15, 16]. It seems that the hole mobility is largely determined by the amount of N atoms and independent of the growth methods. This indicates that the N atoms contribute to the formation of dominant scattering centers. The electrical deterioration has been considered to be caused by the inhomogeneity of the N distribution. Therefore, it may be possible to improve the electrical property by controlling the growth process. In this work, CBE technique was used for the growth of GaAsN. This method has been developed in our group and shown the improvement in the electrical properties [18, 19].

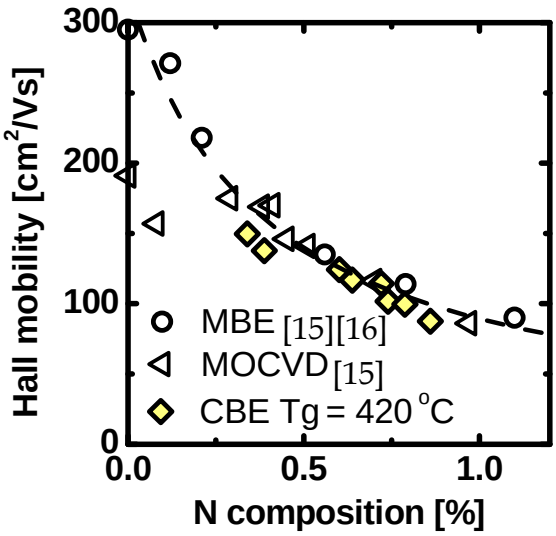

Figure 1. The N composition dependence of the hall mobility of p-GaAsN. The dashed line is a guide for the eye.

In this chapter, the improvement of the carrier mobility and minority carrier lifetime in GaAsN grown by CBE is described. The effects of the growth rate and substrate orientation on these electrical properties are discussed.

2. Chemical beam epitaxy

2.1. Growth procedure of chemical beam epitaxy

The CBE technique has both natures of the metal organic chemical vapor deposition (MOCVD) and molecular beam epitaxy (MBE): metal organic gas sources and low pressure growth [19].

http://dx.doi.org/10.5772/51885

In addition, the growth temperature is lower than the other methods. The low temperature is expected to be advantageous to obtain a non-equilibrium condition and homogeneous distribution of N in As sites. The growth condition of the CBE technique is shown in Table 1. The semi-insulating GaAs(001) oriented in 2° towards [010] was used as the substrate. The growth pressure is around 10^{-2} Pa or below, therefore the mean free path of the source gas molecules is in the order of 10^{-1} m. Triethylgallium [TEGa, Ga(C2H5)3], and monomethylhydrazine [MMHy, (CH3)N2H3], were used as the sources of Ga, and N. Trisdimethylaminoarsenic [TDMAAs, As(N(CH3)2)3] was used as the As source instead of As_2 obtained by cracking As_2H_4. Typical flow rates of TEGa, TDMAAs, and MMHy were 0.1, 1.0, and 9.0 sccm, respectively. The substrate was annealed in the chamber at a temperature of 500 °C for 5 minutes with supplying TDMAAs to remove the oxidized layer on the surface. Then, GaAsN thin film was grown by supplying TEGa and MMHy. The growth temperature was 340 to 460 °C. The growth time was 30 minutes.

Substrate			**Semi-insulating GaAs(001) with 2° offcut toward [010]**	
Growth pressure			2×10^{-2} Pa	
Source	Flow rate (sccm)	Ga	TEGa [$Ga(C_2H_5)_3$]	0.02 - 0.1
		As	TDMAAs [$As(N(CH_3)_2)_3$]	1.0
		N	MMHy [$(CH_3)N_2H_3$]	9.0
Post annealing			5 min. at 500 ℃	
Growth temperature (℃)			340 ~ 480	
Growth time (min.)			30	

Table 1. The growth condition of the CBE technique.

The N composition was estimated from the lattice constant of GaAsN(004) determined by X-ray diffraction (XRD). Here, elastic distortion and Vegard's law were assumed [20]. The growth rate was determined by the film thickness estimated from the interference fringe peaks in an XRD curve and growth time, or the Dektak surface profilometer in the case that no fringe peaks appeared. The crystal quality of the films was evaluated by the full width at half maximum (FWHM) of the rocking curve of a GaAsN(004) peak.

2.2. Growth of GaAsN thin films

The growth temperature dependences of the growth rates are shown in Figure 2. The growth temperature can be divided into three regions. In the lower temperature region (340 – 390 °C), the growth rate increases with increasing temperature. In the middle temperature region (390 – 445 °C), the growth rate decreases with increasing temperature. In the higher temperature region (445 – 480 °C), the growth rate slightly changes. The relationship between the TEGa flow rate and growth rate in each growth temperature region is shown in Figure 3. The growth temperatures of 360, 420, and 480 °C in Figure 3 belong to the low, middle, and high growth temperature regions, respectively. Here, the TDMAAs flow rate was 1.0 sccm and MMHy flow rate was 9.0 sccm. In the case that the growth temperature was 360 °C (in the low temperature

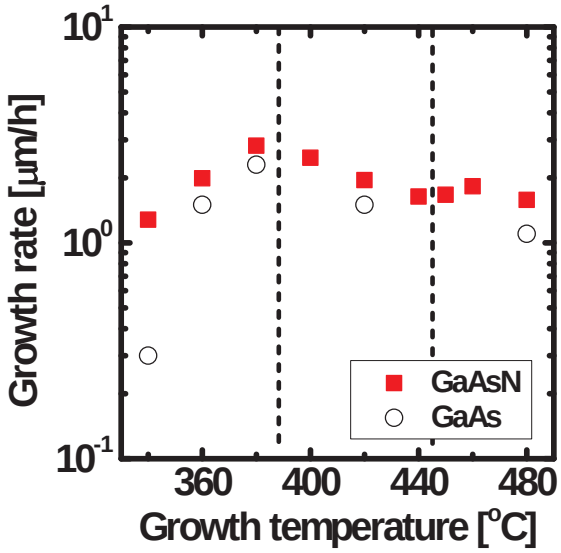

Figure 2. The dependence of the growth rate on the growth temperature of GaAs and GaAsN thin films.

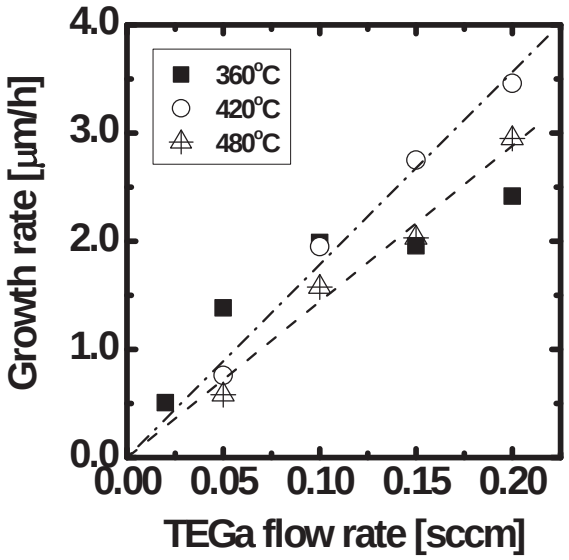

Figure 3. The dependence of TEGa flow rate on the growth rate of GaAsN thin films.

region), the growth rate saturated above the TEGa flow rate of 0.1 sccm. It indicates that the factor that determines the growth rate changed from the TEGa supply to another process such

http://dx.doi.org/10.5772/51885

as the decomposition rate of TEGa on the surface. At higher growth temperatures (in the middle and high temperature regions), the growth rate linearly increased as increasing TEGa flow rate, which indicates that the TEGa supply was dominant to determine the growth rate.

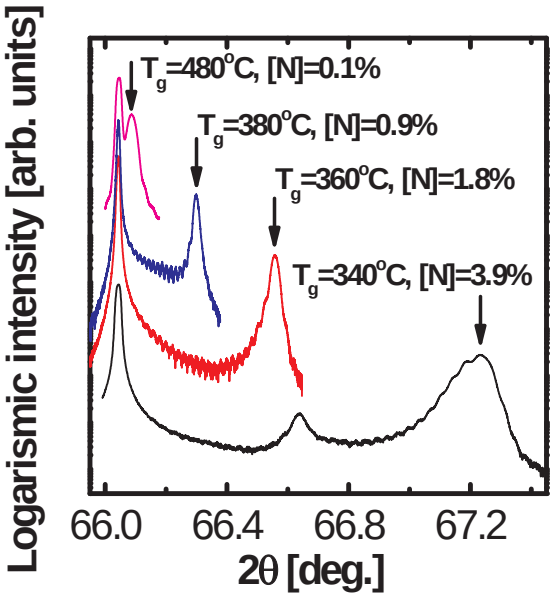

Figure 4. The XRD rocking curves of the GaAsN thin films grown by CBE. The corresponding growth temperature and N composition of each sample is also shown

The XRD rocking curves of GaAsN(004) are shown in Figure 4. The GaAsN films were grown at the temperatures of 340, 360, 380, and 480 °C. There are interference fringes in the rocking curves of the last three films, which suggest the uniformity of the lattice constant with flat interface. On the other hand, there is no fringe in the rocking curve of the film grown at 340 °C, indicating a poor quality of the crystal. The N compositions estimated from the XRD measurements monotonically decreased by increasing the growth temperatures as shown in Figure 5. This is the same tendency as those in the temperature dependence of the growth rate. In the middle region of the growth temperature (390 – 445 °C), the decrement of the N composition is relatively small compared to those in the lower (340 – 390 °C) and higher (445 – 480 °C) regions.

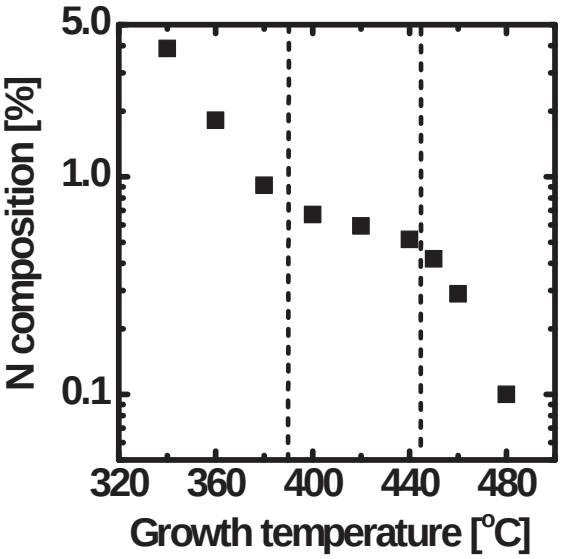

Figure 5. The dependence of growth temperature on the N composition in GaAsN thin films.

2.3. Crystal quality of GaAsN grown by CBE

The FWHM's of measured samples divided by the theoretical calculations of GaAsN(004) peaks are shown in Figure 6. To remove the contribution of the film thickness, those were normalized by using the Schereer's equation. When the film was grown above 360 °C, the ratios are almost 1.0, which indicates good crystal quality. On the other hand, the large ratio of the film grown at 340 °C means poor quality of the crystal, corresponding to no fringe in XRD spectra. This deterioration of the crystal quality possibly occurred due to the incorporation of a large amount of impurities, such as hydrogen and carbon.

The dependence of the N composition on the growth temperature as shown in Figure 5 can be explained qualitatively as follows. A rapid decrease in the N composition with increasing the growth temperature in the low growth temperature region is due to both the increases in the growth rate and desorption rate of N species at the growing surface. Here, we assume that the amount of N species supplied to the growing surface is independent of growth temperatures. Then, the higher growth rate caused the decrement of the N source supply per unit layer growth, since the N source flow rate was constant in every growth conditions. In the middle growth temperature region, the decrement of the growth rate as increasing the growth temperature would enhance the N source supply per unit layer growth. However, the N composition did not increase. It indicates that the desorption rate of N species prevailed in the middle growth temperature region to reduce the N composition as the growth temperature increased. In the high growth temperature region, the N composition again markedly decreases with increasing the growth temperature. The fact that the growth rate remains almost

http://dx.doi.org/10.5772/51885

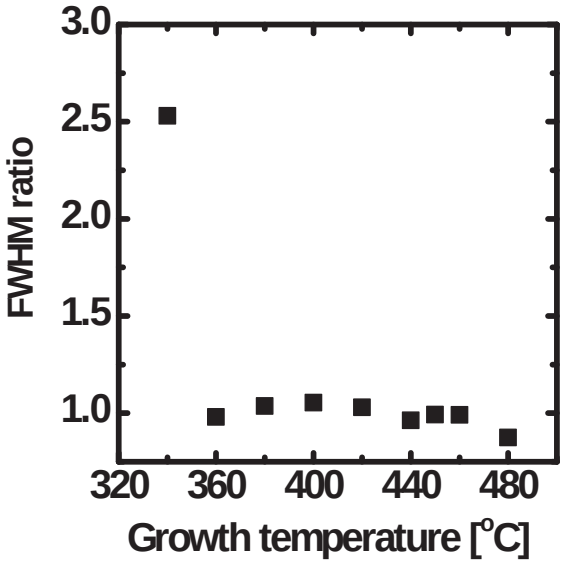

Figure 6. The ratio of FWHM obtained from the measured samples and theoretical calculation at each growth temperature.

constant in that region as shown in Figure 2 indicates that the increased desorption rate of N species are dominant to determine the N composition. Although these three dependences were also observed in the CBE-grown GaAsN with the atomic N source [14], the slope of XRD rocking curves in each region is steeper in our result. This is considered to mainly come from the difference in desorption rate between the N sources on the growing surface. To further understand the N incorporation mechanism in CBE with compound N sources, such as MMHy, it is necessary to consider the desorption rate of N species.

3. Hole mobilities

3.1. Hall hole mobility

The hole mobility in p-GaAsN films grown by CBE, MBE, and MOCVD is shown in Figure 7 as a function of N composition [16, 21]. Those grown by the CBE in our group were obtained by Van der Pauw method. The dashed line represents the mobility obtained theoretically by considering the alloy and phonon scatterings. The hole mobility monotonically decreases as increasing the N composition and they are smaller than the theoretical values. The deviation of the mobility from the ideal value is at the same level despite the different impurity concentrations [16, 21]. This indicates that some N-related defects are generated due to the N incorporation, which determine the hole mobility at the room temperature. To evaluate the number of N-related defects, the temperature dependence (77-400K) of the hole mobility was

obtained as shown in Figure 8. The result suggests that there are several different scattering mechanisms. To determine the amount of the N-related scattering centers, we analyzed this temperature dependence. Here, ionized impurity scattering, alloy scattering, phonon scattering, and N-related carrier scattering were considered [22, 23]. The inverse of the mobility limited by the N-related carrier scattering $1/\mu_N$, which is proportional to the density of N-related scattering centers, was determined by excluding the contributions of the mobility limited by ionized impurity (μ_{II}), alloy scattering (μ_{AL}), and phonon scattering (μ_{PN}) from the measured mobility (μ_{exp}), as follows:

$$\frac{1}{\mu_N} = \frac{1}{\mu_{\exp}} - \frac{1}{\mu_{II}} - \frac{1}{\mu_{AL}} - \frac{1}{\mu_{PN}}. \tag{1}$$

Here, $1/\mu_{PN}$ is the sum of the contributions from the acoustical phonon (μ_{AC}), polar optical phonon (μ_{PO}), and non-polar optical phonon scattering (μ_{NPO}) as

$$\frac{1}{\mu_{PN}} = \frac{1}{\mu_{AC}} + \frac{1}{\mu_{PO}} + \frac{1}{\mu_{NPO}}. \tag{2}$$

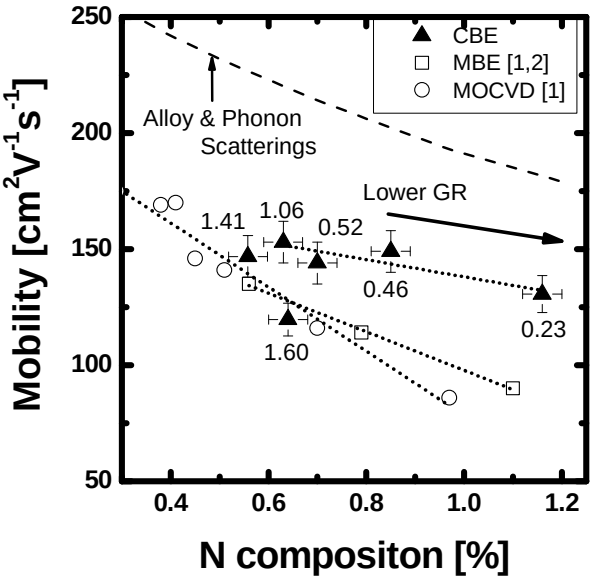

Figure 7. Hole mobility at room temperature in p-GaAsN films grown by CBE, MBE, and MOCVD as a function of N composition. The mobility is the value at room temperature. The dashed line represents the estimated mobility limited by the alloy and phonon scatterings. In the case of CBE, the growth rate (GR) is shown in the unit of μm/h. The dotted lines are a guide for the eye.

http://dx.doi.org/10.5772/51885

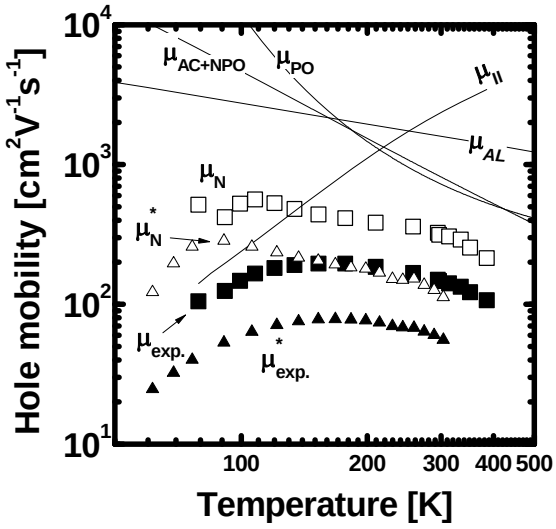

Figure 8. Temperature dependence of the hole mobility of p-GaAsN films with N composition of approximately 0.34% ($\mu_{exp.}$) and its components denoted in eq. (1). The contribution from N-related scattering centers (μ_N) is obtained by using eq. (1). The mobility with N composition of approximately 0.79% ($\mu^*_{exp.}$) and contribution from the N-related scattering centers (μ^*_N) are also shown.

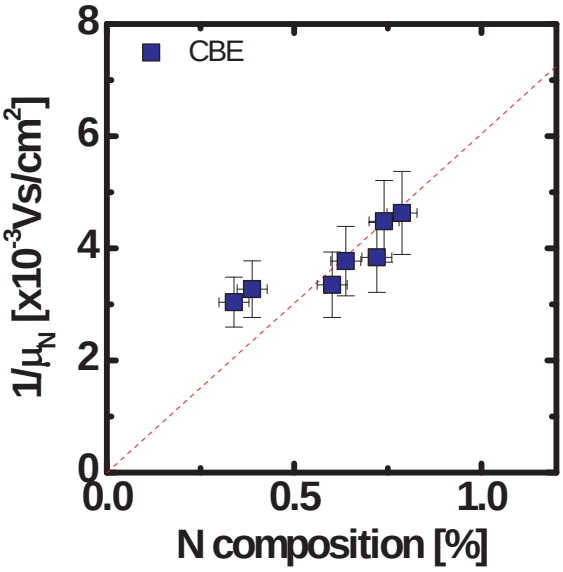

Figure 9. $1/\mu_N$ at each N composition in p-GaAsN films.

The expressions of each component of the mobility are described, for example, in ref. [16].

The relationship between $1/\mu_N$ and N composition is shown in Figure 9. The inverse of the mobility limited by the N-related carrier scattering center ($1/\mu_N$) was determined, which is proportional to the amount of N-related scattering centers. Independent of growth technique, the number of N related scattering centers ($1/\mu_\infty$) increases as N composition increases.

3.2. Improvement of mobility by controlling the growth rate

The above result suggested that the number of N-related defects may be determined by the N concentration of the GaAsN independent of the growth technique. However, here we show the increase of the mobility by controlling the growth rate in CBE. The hole mobility at room temperature and the N composition in p-GaAsN films as a function of growth rate are shown in Figure 10. The higher mobilities are obtained by decreasing the growth rate. Generally, the hole mobility is decreased by the increase in the N composition owing to the alloy scattering. To discuss the reason for the increase in the hole mobility, the relationship between the $1/\mu_N$ and N composition are shown in Figure 11. When the growth rate is higher than 1.41 μm/h, there is no improvement of the mobility. By decreasing the growth rate lower than 1.04 μm/h, the $1/\mu_N$ (the number of the N-related defects) remains almost constant despite the increase in the N composition. $(\mu_N\ [N])^{-1}$ as a function of the growth rate is shown in Figure 12. This is a relative amount of the N-related scattering centers to the total amount of N atoms. $(\mu_N\ [N])^{-1}$ is decreased by decreasing the growth rate monotonically. Then, the controlling growth rate in CBE is effective to suppress the formation of N-related scattering centers and to improve the mobility, especially for a higher N composition.

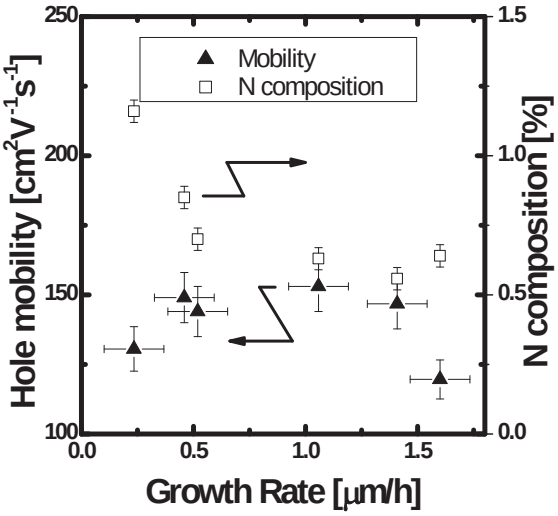

Figure 10. Hole mobility at room temperature and N composition in p-GaAsN films as a function of growth rate.

http://dx.doi.org/10.5772/51885

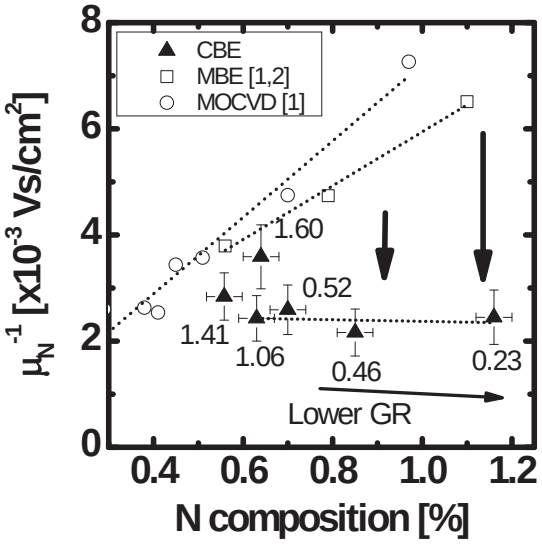

Figure 11. μN-1 at room temperature as a function of N composition in p-GaAsN films. μ_N^{-1} is proportional to the amount of N-ralated scattering centers. In the case of CBE, the growth rate (GR) is shown in the unit of μm/h. The dotted lines are a guide for the eye.

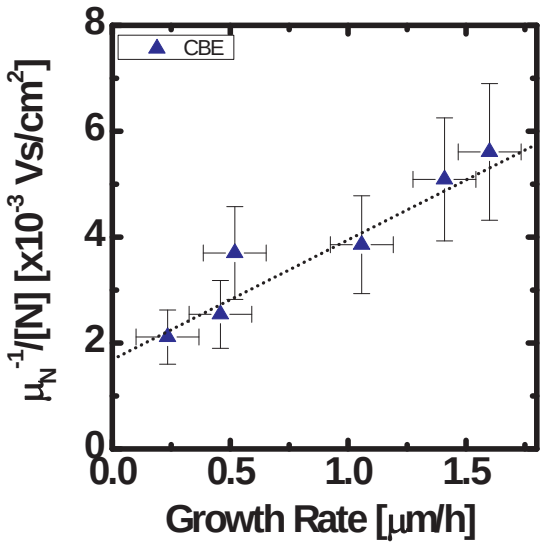

Figure 12. $(\mu_N\ [N])^{-1}$ as a function of growth rate of p-GaAsN films. $(\mu_N\ [N])^{-1}$ is the relative amount of the N-related scattering centers to the total amount of N atoms. The dotted line is a guide for the eye.

We inferred two reasons for the reduction of the amount of N-related scattering centers by decreasing the growth rate: i) The amount of N adsorbed species which are desorbed from a terrace increases by decreasing the growth rate. We expect that the N adsorbed species adsorbed from a terrace is a cause of N-related scattering centers. The desorption from a terrace is expected to be more frequent than that from a step, since the number of connected bonds of N adsorbed species to the growing surface is smaller at terrace than at step; ii) The decrease in the growth rate increases the diffusion length of N adsorbed species on the growing surface. A large diffusion length is expected to increase the probability of a N adsorbed species to come over a step. Therefore, the probability of a N adsorbed species adsorbed at a step increases. Then, i) and ii) are expected to be advantageous for the improvement of the carrier mobility and lifetime.

4. Mobility contributed from N-related scattering center

4.1. Minority-carrier lifetime

4.1.1. Improvement of minority carrier lifetime by controlling growth rate

As the control of the growth rate improved the mobility, here we show that the decreasing the TEGa flow rate improves the minority carrier lifetime.. The minority-carrier lifetime at room temperature was obtained by time-resolved photoluminescence (TR-PL). A titanium sapphire pulse laser was used for the carrier excitation. The excitation power, wavelength, pulse width, and recurrence frequency were 900 mW, 800 nm, ~100 fs, and 80 MHz, respectively. To evaluate the minority carrier lifetime of p-GaAsN, the structure of GaAs buffer layer (500 nm)/ p-GaAsN layer (140~950 nm)/GaAs cap layer (30 nm) was adopted. The cap layer reduced the surface recombination. The PL lifetime (τ_{PL}) was obtained by PL decay curves. τ_{PL} consists of minority-carrier lifetimes in the bulk of the p-GaAsN layer (τ_B) and at GaAs/GaAsN interfaces (τ_S). The contribution of τ_S to τ_{PL} changes as a function of the p-GaAsN layer thickness (d)16) as follows:

$$\frac{1}{\tau_{PL}} = \frac{1}{\tau_B} + \frac{1}{\tau_S} = \frac{1}{\tau_B} + \frac{2S}{d}. \tag{3}$$

Here, S is the GaAs/GaAsN interface recombination velocity. PL lifetime as a function of GaAsN layer thickness was obtained and τ_B was determined by eq. (3). The amount of nonradiative recombination centers were estimated qualitatively based on eq. (4),

$$N_{NR} \propto \frac{1}{\tau_{NR}} = \frac{1}{\tau_B} - \frac{1}{\tau_R}, \tag{4}$$

http://dx.doi.org/10.5772/51885

GR (μm/h)	[N] (%)	τ_B (ns)	τ_R (ns)	τ_{NR} (ns)
2	0.6	3.2×10^{-1}	8.0×10^{1} ($p = 1 \times 10^{17}$ cm^{-3})	3.2×10^{-1}
0.4	0.8	9.0×10^{-1}	1.7×10^{2} ($p = 5 \times 10^{16}$ cm^{-3})	9.0×10^{-1}

Table 2. Summary of growth rate (GR), N composition ([N]), minority-carrier lifetime in the bulk of p-GaAsN (τ_B), and radiative, nonradiative recombination lifetime (τ_R, τ_{NR}). τ_B was estimated by the PL lifetime dependence on the thickness of the p-GaAsN layer. τ_R was determined by using the hole concentration (p). τ_{NR} is obtained by using eq. (3).

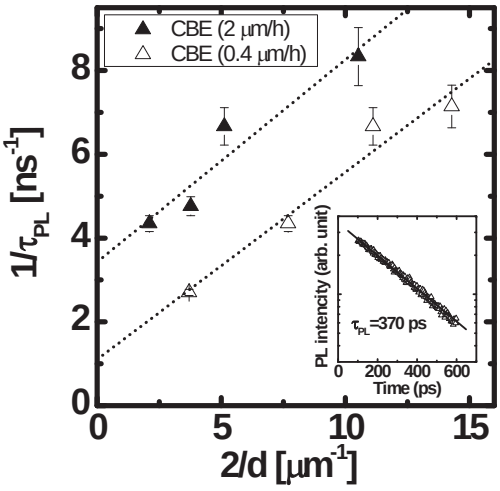

Figure 13. Fitting results of PL lifetime (τ_{PL}) dependence on GaAsN layer thickness (d). The inserted figure shows a typical PL decay curve at room temperature, which is for the sample with GaAsN layer thickness of approximately 500 nm grown at a growth rate of 0.4 μm/h.

where NNR is the density of the nonradiative recombination centers, and τ_{NR} and τ_R are the nonradiative and radiative recombination lifetimes, respectively. τ_R was determined by the hole concentration (p) theoretically.

The decay of PL intensity was shown in Figure 13. The following equation

$$I_{PL}(t) = I_0 \exp\left(-\frac{t}{\tau}\right). \tag{5}$$

explains well about the PL decay curve. Here, $I_{PL}(t)$ is the PL intensity at the time t, and I_0 is the PL intensity at t = 0, just after the carriers are excited. The lifetime τ obtained by eq. (5) is the PL lifetime (τ_{PL}) in eq. (3). To estimate the minority-carrier lifetime in the bulk of the p-

GaAsN layer (τ_B), τ_{PL} dependence on GaAsN layer thickness (d) was obtained (Figure 13). When the growth rate was 2 μm/h, τ_B was 3.2 x 10^{-1} ns ([N] = 0.6%). By decreasing the growth rate to 0.4 μm/h, τ_B was increased to 9.0 x 10^{-1} ns ([N] = 0.8%) despite the increase in the N composition. Therefore, decreasing the growth rate in CBE is effective to improve τ_B. Further, the improvement is more effective when the N composition is higher.

The density of the nonradiative recombination centers determines the nonradiative recombination lifetime (τ_{NR}). To discuss the amount of nonradiative recombination centers, τ_{NR} is estimated by eq. (4). The recombination lifetime (τ_R) depends on the hole concentration (p), as follows:

$$\tau_R = \frac{1}{Bp}. \tag{6}$$

Here, B is the radiative recombination probability,

$$B = 0.58 \times 10^{-12} \sqrt{\varepsilon} \left(\frac{1}{m_p^* + m_n^*} \right)^{1.5} \times \left(1 + \frac{1}{m_p^*} + \frac{1}{m_n^*} \right) \left(\frac{300}{T} \right)^{1.5} E_g{}^2, \tag{7}$$

where ε is the dielectric constant, m_p^* and m_n^* are the hole and electron effective masses, respectively, in units of the free electron mass, T is the temperature, and E_g is the band gap. For the p-GaAsN layers discussed here, B calculated by eq. (7) was 1.2 x 10-10 cm3/s. When the growth rate was 2 μm/h, the carrier concentration was 1 x 1017 cm-3. By decreasing the growth rate to 0.4 μm/h, it was decreased to 5 x 1016 cm-3. From eqs. (4) and (6), τ_{NR} and τ_R were obtained to be τ_{NR} = 3.2 x 10-1 ns and τ_R = 8.0 x 101 ns for the growth rate of 2 μm/h, and τ_{NR} = 9.0 x 10-1 ns and τ_R = 1.7 x 102 ns for the growth rate of 0.4 μm/h. These results are summarized in Table 2. Since τ_{NR} is much smaller than τ_R, τ_B is mainly determined by τ_{NR}. Therefore, the improvement of τ_B is mainly due to the increase in τ_{NR}. These results suggest that decreasing the growth rate in CBE is effective to suppress the formation of nonradiative recombination centers and to improve the carrier lifetime. Then, CBE is highly expected to realize the minority-carrier lifetime of more than 1 ns and the diffusion length of more than 1 μm with the target value of the N composition (3%).

4.2. Improvement of minority carrier lifetime by controlling substrate orientation

The effect of the surface orientation on the minority carrier lifetime is studied. GaAsN films were grown on GaAs(311)A, (311)B, and (100) substrates. The (311) surface consists of (111) and (100) components. The surface configurations of the (311)A and (311)B surfaces are shown in Figure 14. On the (311)A surface, a Ga atom connects to three As atoms, while an As atom

http://dx.doi.org/10.5772/51885

connects to two Ga atoms. The same bond configuration holds for the (311)B surface by exchanging Ga and As atoms.

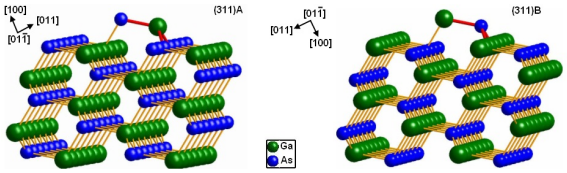

Figure 14. The surface structures of GaAs(311)A (left figure) and (311)B (right figure) substrates. Green balls are Ga atoms, blue balls are As atoms, and yellow and red sticks are Ga-As bonds.

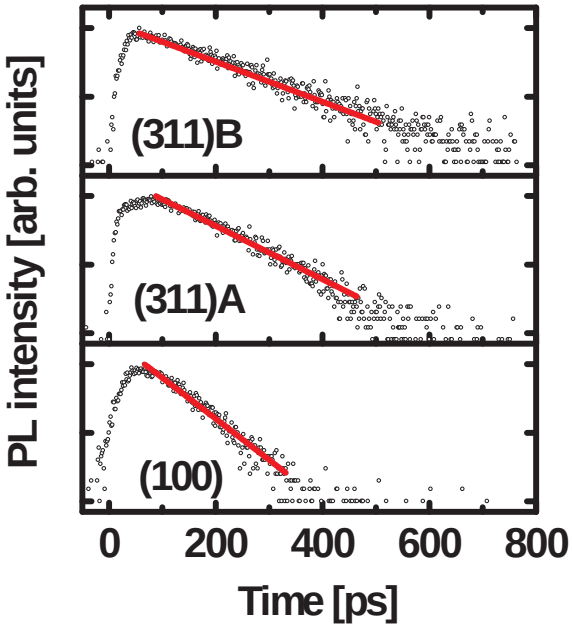

Figure 15. Typical PL decay curves at 4.5K of GaAsN with different growth orientations. The growth temperature was 440 ℃.

The results of the TR-PL measurements at 4.5K of GaAsN films with each growth orientation are shown in Figure 15. The PL lifetime is estimated by approximating the decay curve of the PL intensity as a straight line. The film with (311)B orientation has a longer PL lifetime, which indicates the longer minority carrier lifetime. The PL spectra at 4.5K of as-grown films with various substrate orientations are shown in Figure 16(a). The growth temperature was 440 ℃. There are two GaAsN-related peaks denoted as BE (near-band edge) and DL (deep levels) and

one GaAs-related peaks in the spectra. The GaAsN-related peaks are in the range of 1.25 – 1.40 eV and 1.1 – 1.2 eV which are caused by BE and DL emissions, respectively. To understand the orientation-dependent photoluminescence of GaAsN films, the ratio of the integrated intensities of DL to BE (P_{DL}/P_{BE}) were calculated. The P_{DL}/P_{BE} ratio of the film grown on (311)A had the lowest value at any growth temperatures as shown in Figure 16 (b). The film grown on (311)A has almost the same N composition as that of (100). Therefore, N composition is not related to the difference in the integrated intensity ratios. This result indicates that the high-index substrate surfaces contribute to reduce defects and composition fluctuations in the epilayers [24]. On the other hand, in contrast to the continuous increase in total emission intensities of (3 1 1)B sample, a decreasing tendency with a rise in growth temperature was recorded for (3 1 1)A.

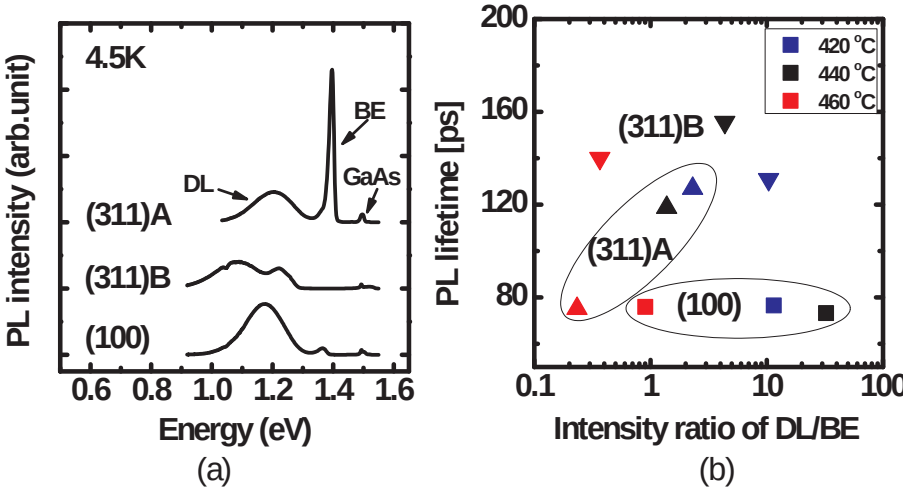

Figure 16. (a) PL spectra at 4.5K of as-grown films with different substrate orientations. The growth temperature was 440 ℃. (b) Growth-temperature dependences of N composition in GaAsN layers on (3 1 1)A/B and (1 0 0) substrates.

5. Lattice defects in GaAsN grown by CBE

GaInAsN suffers from three main N-related problems: (i) the shortening lifetime of minority carriers, (ii) the lowering of their mobility, and (iii) the increase of carrier concentration with increasing N concentration in the alloy [25-27]. Indeed, the incorporation of a small atomic fraction of N in the lattice of GaAs gives rise to the formation of high density acceptor states, recombination centers, and scattering levels [28]. It is; therefore, clear that the degradation of electrical properties of GaAsN may be attributed only to the formation of lattice defects. These defects were expected to be formed during growth owing to the smaller atomic size of N than of As, as well as, to the large gap miscibility between GaAs and GaN. For that, extensive works

http://dx.doi.org/10.5772/51885

on the distribution of lattice defects in the forbidden gap of Ga(In)AsN and their effects on their electrical properties were published during the last decade. Indeed, the summary of experimental results reported by Geisz and Friedman provides a basic knowledge of these defects [4]. Furthermore, undoped Ga(In)AsN alloys grown by chemical compound sources present a high density of residual impurities [29]. This property is a hindrance to a flexible design of Ga(In)AsN based solar cell and reduces the lifetime of minority carriers. Despite the very interesting results about the distribution of lattice defects in GaAsN, the main causes of short diffusion length of minority carriers and high background doping are still elusive. In this section of the chapter, we summarize the distribution of energy states in the forbidden gap of GaAsN grown by CBE, which was obtained using deep level transient spectroscopy and some related methods. Furthermore, we report the relationship of some defects and the poor electrical properties of the alloy, as well as, our recent results to decrease their impacts. All GaAsN samples were grown by CBE on GaAs (100) 2° off toward (110) substrate, under a growth temperature and a pressure of 420-460 °C and 2×10^{-2} Pa, respectively. TEGa, TDMAAs, and MMHy were used as Ga, As, and N chemical compound sources, respectively. SiH_4 was used as n-type doping source, whereas undoped films are p-type. The detail of growth conditions using CBE can be found elsewhere [30-33]. The N concentration in each sample were evaluated from the Bragg angles of the GaAs and GaAsN reflection obtained by high resolution X-ray diffraction (HRXRD) method. The Schottky and ohmic contacts were evaporated through metal masks at a vacuum pressure of 10^{-4} Pa. The free donor and acceptor concentrations were calculated by the fitting of the Mott-Schottky plot using the capacitance-voltage method. DLTS spectra were collected using a BIO-RAD digital DLTS system (DL8000). The activation energies Ea [Ev + ET (eV)] for hole traps and Ea [EC - ET (eV)] for electron trap were determined from the slope of the Arrhenius plot of the DLTS signals, whereas the capture cross sections n/p (cm2) were evaluated from the intercept values [34]. Illustrated in Figure 17 (a) is the distribution of energy states in the forbidden gap of GaAsN0.005 grown by CBE. The main electron and hole traps in GaAsN were recorded by DLTS method and shown in Figure 17 (b) and (c). For electrons traps, two peaks (E1) and (E2) were observed in as grown film around 150 and 300 K, respectively. After rapid thermal annealing, E2 disappears completely and a new electron trap (E3) appears at 200 K. Compared with the electron traps in N-free GaAs, only E1 appears after the introduction of a small amount of N. Therefore, we have strongly suggested that E2 and E3 could be considered as native defects in GaAs. Based on the classification of electron traps in GaAs by Maunitton et al., E2 and E3 were considered to be EL2 (+/0) and EL5, respectively [35]. On the other hand, three hole traps, labeled H0, H2, and H5 were commonly observed in the DLTS spectrum of Figure 17 (c). Compared with the hole traps in N-free GaAs, we could only attribute H5 to the double donor state of EL2 with the charge state (+/++) [36], however, H2 and H0 appear to be newly observed. The hole trap H0 was confirmed to be a radiative recombination center using single and double carrier pulse DLTS method [30]. Since, our interest is only on the N-related defects which could be correlated with the poor electrical properties and the high carrier density in the alloy, we will focus only on the electron trap E1 and the hole trap H2, which were confirmed to be the main cause of the shortening of minority carrier lifetime and the high background doping in GaAsN films,

respectively. The properties of these two defects are summarized respectively in the two next sub-sections.

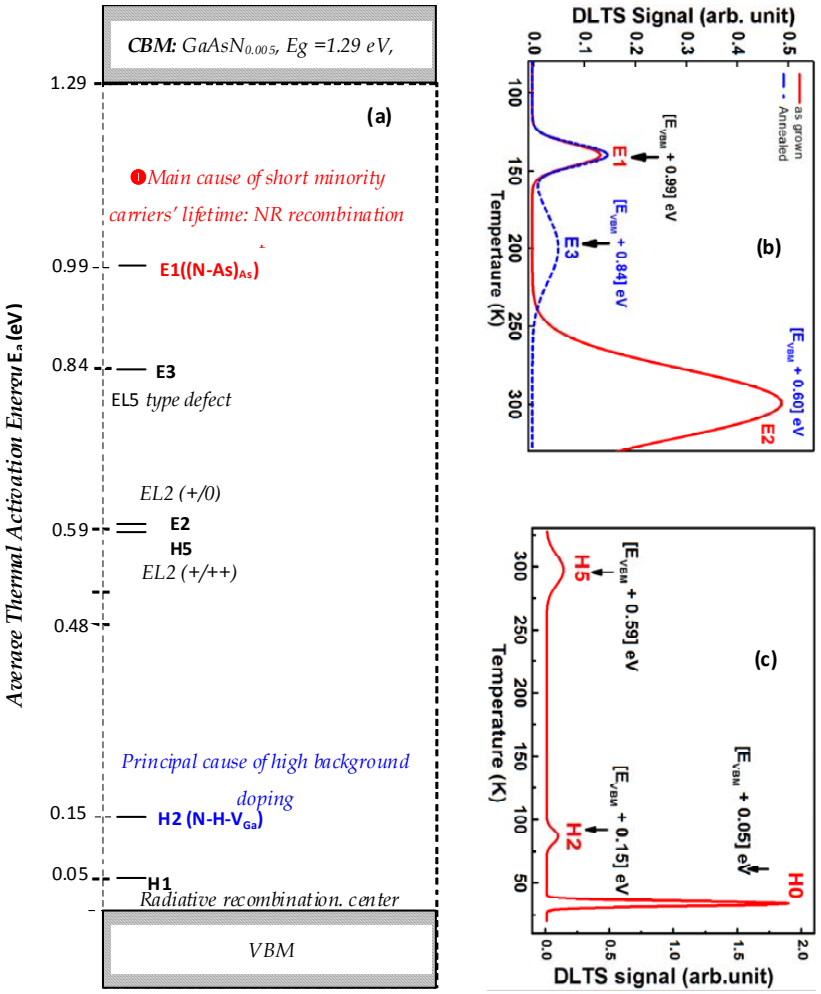

Figure 17. (left) Distribution of lattice defects in GaAsN grown by CBE for a N concentration of 0.5%, DLTS spectra for (a) as grown and annealed GaAs, (b) as grown GaAsN, (c) annealed GaAsN, (d) Arrhenius plot for electron traps, (e) DLTS spectrum for hole traps in GaAsN, and (f) Arrhenius plot for hole traps.

5.1. N-related non radiative recombination center

The electron trap E1 was confirmed to be related to the N atom, since its density increases with increasing the N concentration in GaAsN films [31]. Furthermore, it was not

http://dx.doi.org/10.5772/51885

observed in N-free GaAs [31]. The activation energy of E1 was found to vary between 0.3 and 0.4 eV below the conduction band minimum (CBM) [31-33]. This variation in energy level was explained by the effect of the electrical field on the thermal emission of carriers from E1, since the carrier concentration in GaAsN was not identical in all studied samples [4]. In addition, E1 was not only observed in CBE grown GaAsN but also in the DLTS spectra of MOCVD and MBE grown GaAsN and InGaAsN [37, 38]. Moreover, E1 approximately exhibited similar density and tendency with varying the N concentration, despite the quite difference in residual carrier densities between the three growth methods [31, 38, 39]. This result implies that the possible structure of E1 is independent of impurities. The thermal capture cross section of E1 is too large compared with that of native defects in GaAs. For that, it was found that the DLTS peak height of E1 saturates promptly with increasing the time of injection of electrons through the filling pulse parameter [33]. In view of the effective role of E1 in the degradation of electrical properties of GaAsN, we were able to provide evidence that E1 trap plays a major role in the degradation of minority carrier lifetime and acts as a recombination center [33]. For this, we carried out an experiment based on minority carrier capture at majority carrier trap by double carrier pulse DLTS method [30]. In this experiment, E1 was filled with majority carriers during the first pulse, so that E1 centers are occupied with electrons. Then, a forward bias minority carrier injection of short duration was applied in order to introduce capture of minority carriers. When the junction returned of quiescent reverse bias, E1 centers that remained occupied with majority carriers were emptied by thermal emission. The amplitude of this thermal emission provides a measure of the number of carriers that were trapped by E1 and not filled with minority carriers at the end of the injection pulse. A decrease of E1 peak height was observed and confirmed with varying the rate of injection through the duration and the voltage of the second pulse [33]. This result, indeed, indicates that E1 is a recombination center [33]. After this step, it was essential to identify the nature of this recombination mechanism. For that, the temperature dependence of the capture cross section of E1 (σ_{E1}(was investigated. As known in DLTS measurements, varying the emission rate window shifts the peak of the defect and the capture cross section may change. From the Arrhenius plots of each emission rate, we established the relationship between σ_{E1} and the reciprocal temperature [33]. Absolutely, the recombination process through E1 was confirmed to be nonradiative, since σ_{E1} presents a thermal activation energy of 0.13 eV [33]. Furthermore, σ_{E1} was evaluated at room temperature to around 10^{-13} cm^2 [33]. This result proves that E1 is an active recombination center. In addition, this recombination activity may rises with increasing N in the film, since the activation energy of E1, comes closer to the midgap, following the decrease of the conduction band minimum. The recombination mechanism through E1 was quantified by evaluating the lifetime of electrons from the conduction band the energy level of the electron trap in the forbidden gap of the alloy. Using the SRH model for generationrecombination, the lifetime of electrons from the CBM to E1 was calculated to 0.2 ns [33-39]. This value was experimentally verified by time-resolved photoluminescence measurements. We, therefore, suggest that E1 is the main cause of short minority carrier lifetime in GaAsN alloys.

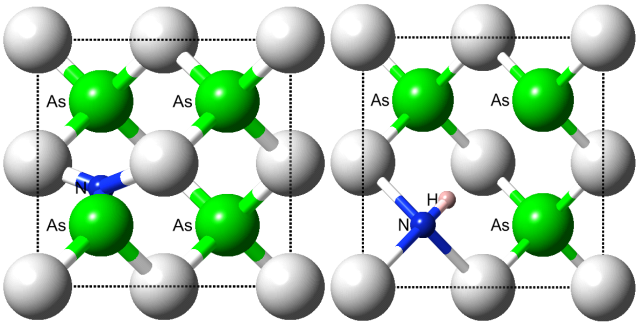

Figure 18. The split intestinal $(N\text{-}As)_{As}$ (left) and $N\text{-}H\text{-}V_{Ga}$ (right) as a possible origins of E1 and H2, respectively.

To understand the formation process of E1 and limit its effect, it was necessary to investigate its origin. First, it was mentioned above that E1 is independent of impurities, such as H, O, and C. Furthermore, E1 was observed in undoped p-type (minority carrier trap), n-type, and Si-doped GaAsN films, which exclude the doping atom from its origin. Therefore, E1 was tentatively suggested to be sensitive only to the host atoms (N, As, and Ga). In addition, using the isothermal capacitance transient method, the density profiling of E1 was found to be quasi-uniform distributed GaAsN [31]. This result indicates that the formation of E1 starts and goes on with the growth process. An obvious reason of this behavior is the compensation for the tensile strain, which could be caused by the small atomic size of N compared with that of As. Theoretically, the split interstitials $(N\text{-}As)_{As}$ and $(N\text{-}N)_{As}$ were expected to form two electron traps at 0.4 and 0.6 eV below the CBM of GaAsN, respectively [40]. These two defects were qualified to be energetically favorable on the growth surface [40]. As the N-dependence of the density of E1 did not show a straight line and since the total N concentration in the film could not be obtained using HRXRD measurements, we have proceed to investigate the relationship between the density of E1 and the flux of the As source. Indeed, we found that the density of E1 shows a peaking behavior with increasing TDMAAs [41]. This result implies that the formation of E1 is sensitive to both N and As atoms. However, this relationship could not be quantified since the atomic fractions between As and N in GaAsN films are quite different [41]. As shown in Figure 18, the split interstitial $(N\text{-}As)_{As}$ is, therefore, expected to be the possible origin for E1. However, more experiments are required to clarify the formation process of this recombination center and to limit its density.

5.2. N-related acceptor like state in GaAsN

The high background doping in undoped GaAsN films is a serious problem for solar cell design and fabrication. A small atomic fraction of N changes the conductivity in the film from n-type in GaAs to p-type. Obviously, the formation of N-related acceptors with high density is the main reason of donor compensation. Indeed, two acceptor levels, A1 and A2, were confirmed using Hall Effect measurements [42]. Their thermal activation energies were evaluated to $E_{A1} = 130 \pm 20$ meV and $E_{A2} = 55 \pm 10$ meV, respectively. On another hand, the ionized acceptor density N_A,

http://dx.doi.org/10.5772/51885

obtained using capacitance voltage (C-V) method, showed a linear dependence with N concentration in undoped films grown under a Ga flow rate of TEGa = 0.1 sccm [32]. This indicates that N_A depends strongly on a N-related acceptor [32]. However, this linear dependence tends to saturate when TEGa is reduced, even the N concentration is enhanced [32]. The reason of this saturation was clarified using SIMS measurements, where the concentration of H impurity decreases slightly with decreasing TEGa [32]. Hence, this result implies that N_A depends strongly to N and H atomic concentrations in the film. To identify this N-H related acceptor level, we carried out C-V measurements in the temperature range 20 - 330 K in order to get the temperature dependence of N_A. A sigmoid increase of N_A was observed between 70 and 100 K [32]. Its amplitude showed a strong dependence with N concentration [32]. It approximately reflects the relationship between N_A and N concentration at room temperature [39]. This result indicates that the sigmoid increase of N_A between 70 and 100 K is owing to the thermal ionization of a N-related acceptor-like state, which thermal ionization energy can be estimated to be between 0.1 and 0.2 eV. Furthermore, as given in Figure 17 (c), the hole trap H2 was observed in the temperature range of sigmoid increase of N_A. The activation of H2 is within the expected range of the N-related acceptor state and it is in conformity with theoretical calculation [32, 44]. Furthermore the density of H2 was found to be in linear dependence with N concentration in the samples grown under TEGa = 0.1 sccm. Hence, H2 is suggested to be the main acceptor state which governs the tendency of N_A and it is the cause of the increase of junction capacitance in the temperature range 70 to 100 K. The origin of H2 was investigated using the results of carrier concentration and the density of residual impurities in undoped GaAsN grown by CBE under various Ga flow rates, obtained using Hall Effect, FT-IR, and SIMS [32, 42]. From SIMS measurements, which were carried out on GaAsN grown under different TEGa flow rates, it was found that N_A depends on the atomic concentrations of N and H [32, 42]. In addition, using FTIR measurements, a linear relationship was established between the concentration of N-H complexes and N concentration [29]. Therefore, H2 was strongly suggested to be an acceptor state and its origin is related to the N-H bond. However, the slope of the linear relationship between N_A and the concentration of N-H complexes showed an increase with increasing the growth temperature ($T_G \in [400, 430]$ C) [29]. This indeed indicates that the N-H complexes could be accompanied with another defect, which binding energy was evaluated to 2.5 eV [29]. On another hand, using theoretical calculation, the formation energy of $(N\text{-}H\text{-}V_{Ga})^{-2}$ was found to be lower than $(N\text{-}V_{Ga})^{-3}$, $(H\text{-}V_{Ga})^{-2}$, and isolated V_{Ga}^{-3} [43]. These results may expect V_{Ga} as a possible origin of the unknown intrinsic defect. These predictions were experimentally supported using positron annihilation spectroscopy results [44]. Therefore, H2 may have $N\text{-}H\text{-}V_{Ga}$ as a possible structure as shown in Figure 18.

6. Conclusion

InGaAsN is a candidate material to realize the ultrahigh efficiency multi-junction solar cell. The efficiency of the 4-junction solar cell, InGaP/InGaAs/InGaAsN/Ge, is expected to be 41% under 1-sun (AM0) and 52% under 500-sun (AM1.5). In order to achieve the expected super high efficiency, the electrical property of the InGaAsN should be improved. In this paper, we have shown the following results:

1. The CBE method was developed for the growth of GaAsN films. The growth temperature region was divided into three parts. In the middle growth temperature region (390 – 445 °C), the higher N composition without broadening of the XRD rocking curve width was obtained. In this temperature region, a typical characteristics in the growth process is that the amount of the N incorporation into crystal at the surface is not only dominated by the growth rate but also the desorption rate of N species at the surface.

2. Decreasing the growth rate was effective to improve the hole mobility and minority-carrier lifetime in p-GaAsN films grown by the chemical beam epitaxy (CBE). The mobility was increased from 120 to 150 $cm^2V^{-1}s^{-1}$ for the N composition of 0.6%. Based on the temperature dependence of the mobility, μ_N, which was inversely proportional to the amount of N-related scattering centers, was estimated. By decreasing the growth rate, μ_N^{-1} was reduced especially when the N composition was higher. The result indicates the improved mobility by decreasing the N-related scattering centers. The minority-carrier lifetime in the bulk of p-GaAsN films, τ_B, estimated by PL decay curves was improved from 3.2×10^{-1} ([N] = 0.6%) to 9.0×10^{-1} ns ([N] = 0.8%) despite the higher N composition. The bulk minority-carrier lifetime τ_B was mainly determined by the nonradiative recombination lifetime (τ_{NR}). This means that the nonradiative recombination centers were reduced by decreasing the growth rate, which resulted in the improvement of τ_B.

3. The electron lifetime of p-GaAsN was also improved by controlling the GaAs substrate orientations. The investigation of the effects from GaAs substrate surface orientation and polarity indicates that N incorporation can be enhanced on the (3 1 1)B plane but reduced on (3 1 1)A compared with (1 0 0), where the three dangling bond sites on the (3 1 1) growing surface are considered to play the dominant role. The examination of intensity ratio between emissions from band edge and deep levels evidenced the improved luminescence efficiency of GaAsN layers on (3 1 1) substrates with both polarity. In response to variations in the growth temperature and the postgrowth annealing, optical behavior shows strong dependence on the epitaxial orientation, as illustrated by the relative intensity and low-energy tail of the band-edge emission. (3 1 1)B is distinguished to be the potential substrate to achieve efficient N incorporation.

4. The electron trap E1 located at 0.99 eV above VBM is a dominant non radiative recombination center. The formation of E1 is sensitive to both the amounts of N and As atoms. A possible structure of this defect is $(N\text{-}As)_{As}$. The hole trap H2 located at 0.15 eV above VBM is suggested to be the main acceptor state. The origin of H2 is related to the N-H bond. A possible structure is $N\text{-}H\text{-}V_{Ga}$.

Author details

Kazuma Ikeda, Han Xiuxun, Bouzazi Boussairi and Yoshio Ohshita

Toyota Technological Institute, Japan

References

[1] Kondow M, Uomi K., Niwa A, Kitatani T, Watahiki S, Yazawa Y, GaInNAs: A novel material for long-wavelength-range laser diodes with excellent high-temperature performance. Japanese Journal of Applied Physics 1996; 35 1273–1275. DOI: 10.1109/2944.640627.

[2] Bellaiche L. Band gaps of lattice-matched (Ga,In)(As,N) alloys. Applied Physics Letters 1999; 75 2578-2580. DOI: 10.1063/1.125083.

[3] Green MA, Emery K, Hishikawa Y, Warta W, Dunlop ED. Solar cell efficiency tables (version 39). Progress in Photovoltaics: Research and Applications 2012;20 12-20. DOI: 10.1002/pip.

[4] Geisz JF, Friedman DJ. III–N–V semiconductors for solar photovoltaic applications. Semiconductor Science and Technology 2002; 17 769–777.

[5] Dimroth F, Baur C, Bett A, Volz K, Stolz W. Comparison of dilute nitride growth on a single-and 8×4-inch multiwafer MOVPE system for solar cell applications. Journal of Crystal Growth 2004;272 726–731. DOI: 10.1016/j.jcrysgro.2004.08.038.

[6] Neugebauer J, Van de Walle CG. Electronic structure and phase stability of $GaAs_{1-x}N_x$ alloys. Physical Review B 1995;51 10568–10571. DOI: 10.1103/PhysRevB.51.10568.

[7] Pan Z, Li LH, Zhang W, Lin YW, Wu RH. Kinetic modeling of N incorporation in GaInNAs growth by plasma-assisted molecular-beam epitaxy. Applied Physics Letters 2000;77 214-216. DOI: 10.1063/1.126928.

[8] Zhongzhe S, Fatt YS, Chuin YK, Khai LW, Weijun F, Shanzhong W, Khee NT. Incorporation of N into GaAsN under N overpressure and underpressure conditions. Journal of Applied Physics 2003; 94 1069-1073. DOI: 10.1063/1.1582554.

[9] Ougazzaden A, Bellego YL, Rao EVK, Juhel M, Leprince L, Patriarche G. Metal organic vapor phase epitaxy growth of GaAsN on GaAs using dimethylhydrazine and tertiarybutylarsine. Applied Physics Letters 1997;70(21) 2861-2863. DOI: 10.1063/1.119025.

[10] Dumont H, Auvray L, Monteil L, Bouix J. Analysis of nitrogen incorporation mechanisms in GaAs1−xNx/GaAs epilayers grown by MOVPE. Materials Science and Engineering: B 2001;84(3) 258-264. DOI: 10.1016/S0921-5107(01)00639-0.

[11] Kurtz S, Reedy R, Keyes B, Barber GD, Geisz JF, Friedman DJ, McMahon WE, Olson JM. Evaluation of NF3 versus dimethylhydrazine as N sources for GaAsN. Journal of Crystal Growth 2002;234 323-326. DOI: 10.1016/S0022-0248(01)01712-2.

[12] Jin C, Nikishin SA, Kuchinskii VI, Temkin H, Holtz M. Metalorganic molecular beam epitaxy of (In)GaAsN with dimethylhydrazine. Journal of Applied Physics 2002;91 56-64. DOI: 10.1063/1.1419206.

[13] Uesugi K, Suemune I. Metalorganic molecular beam epitaxy of GaNAs alloys on (0 0 1)GaAs. Journal of Crystal Growth 1998;189–190 490-495. DOI: 10.1016/S0022-0248(98)00337-6.

[14] Sun Y, Yamamori M, Egawa T, Ishikawa H. Incorporation of N into GaAsN under N overpressure and underpressure conditions. Japanese Journal of Applied Physics 2004;43 2409-2413. DOI: 10.1143/JJAP.43.2409.

[15] Ptak AJ, Johnston SW, Kurtz S, Friedman DJ, Metzger WK. A comparison of MBE- and MOCVD-grown GaInNAs. Journal of Crystal Growth 2003;251 392-398. DOI: 10.1016/S0022-0248(02)02201-7.

[16] Matsuura T, Miyamoto T, Makino S, Ohta M, Matsui Y, Koyama F. p-Type Doping Characteristics of GaInNAs:Be Grown by Solid Source Molecular Beam Epitaxy. Japanese Journal of Applied Physics 2004;43 L433-L435. DOI: 10.1143/JJAP.43.L433.

[17] Fahy S, O'Reilly EP. Intrinsic limits on electron mobility in dilute nitride semiconductors. Applied Physics Letters 2003;83 3731-3733. DOI: 10.1063/1.1622444.

[18] Yamaguchi M, Warabisako T, Sugiura H. Chemical beam epitaxy as a breakthrough technology for photovoltaic solar energy applications. Journal of Crystal Growth 1994;136 29-36. DOI: 10.1016/0022-0248(94)90379-4.

[19] Lee HS, Nishimura K, Yagi Y, Tachibana M, Ekins-Daukes NJ, Ohshita Y, Kojima N, Yamaguchi M. Chemical beam epitaxy of InGaAsN films for multi-junction tandem solar cells. Journal of Crystal Growth 2005; 275 e1127-e1130. DOI: 10.1016/j.jcrysgro.2004.11.200.

[20] Tsang WT, From Chemical Vapor Epitaxy to Chemical Beam Epitaxy. Journal of Crystal Growth 1989;95 121-131. DOI: 10.1016/0022-0248(89)90364-3.

[21] Uesugi K, Morooka N, Suemune I. Reexamination of N composition dependence of coherently grown GaNAs band gap energy with high-resolution x-ray diffraction mapping measurements. Applied Physics Letters 1999;74 1254-1256. DOI: 10.1063/1.123516.

[22] Wiley JD., Mobility of Holes in III-V Compounds. In: Willardson RK, Beer AC. (ed.) Semiconductors and Semimetals. New York: Academic Press; 1975;10 p. 91-174.

[23] Nag BR. Electron Transport in Compound Semiconductors. Berlin Heidelberg: Springer-Verlag; 1980.

[24] Moto A, Takahashi M, Takahashi S. Effect of Substrate Orientation on Photoluminescence of GaNAs. Japanese Journal of Applied Physics 2000 39;1267-1269.

[25] Buyanova IA., Chens WM. Physics and Applications of Dilute Nitrides, New York: Taylor & Francis Books Inc.; 2004.

[26] Henini M. Dilute Nitrides, Oxford: Elsevier; 2005.

[27] Shan W, Walukiewicz W, Ager J, Haller EE, Geisz JF, Friedman DJ, Olson JM, Kurtz SR. Physical Review Letters 1999;82 1221-1224.

[28] Kurtz SR, Meyers D, Olson JM, Conference Record of the Twenty-Sixth IEEE: conference proceedings, September 29-October 3, 1997, Anaheim Marriott, California, USA. 26th IEEE Photovoltaic Specialists Conference; 1997.

[29] Nishimura K, Suzuki H, Saito K, Ohshita Y, Kojima N, Yamaguchi M. Electrical properties of GaAsN film grown by chemical beam epitaxy. Physica B: Condensed Matter 2007;401 343-346. DOI: 10.1016/j.physb.2007.08.183.

[30] Bouzazi B, Suzuki H, Kojima N, Ohshita Y, Yamaguchi M, A recombination center in p-type GaAsN grown by chemical beam epitaxy. Solar Energy Materials and Solar Cells 2011; 95 281-283. DOI: 10.1016/j.solmat.2010.04.047.

[31] Bouzazi B, Suzuki H, Kojima N, Ohshita Y, Yamaguchi M. Nitrogen Related Electron Trap with High Capture Cross Section in n-Type GaAsN Grown by Chemical Beam Epitaxy. Applied Physics Express 2010;3 0510021. DOI: 10.1143/APEX.3.051002.

[32] Bouzazi B, Suzuki H, Kojima N, Ohshita Y, Yamaguchi M. Nitrogen-Related Recombination Center in GaAsN Grown by Chemical Beam Epitaxy. Japanese Journal of Applied Physics 2010;49 051001. DOI: 10.1143/JJAP.49.051001.

[33] Bouzazi B, Suzuki H, Kojima N, Ohshita Y, Yamaguchi M. Double carriers pulse DLTS for the characterization of electron-hole recombination process in GaAsN grown by chemical beam epitaxy. Physica B: Condensed Matter 2011;406 1070-1075. DOI: 10.1016/j.physb.2010.11.086.

[34] Lang DV. Deep-level transient spectroscopy: A new method to characterize traps in semiconductors. Journal of Applied Physics 1974;45 3023-3032. DOI: 10.1063/1.1663719.

[35] Martin GM, Mitonneau A, Mircea A. Electron traps in bulk and epitaxial GaAs crystals. Electronics Letters 1977;13 191-193. DOI: 10.1049/el:19770140.

[36] Bouzazi B, Nishimura K, Suzuki H, Kojima N, Ohshita Y, Yamaguchi M. Properties of Chemical Beam Epitaxy grown $GaAs_{0.995}N_{0.005}$ homo-junction solar cell. Current Applied Physics 2010;10 S188-S190. DOI: 10.1016/j.cap.2009.11.020.

[37] Johnston SW, Kurtz SR. Comparison of a dominant electron trap in n-type and p-type GaNAs using deep-level transient spectroscopy. Journal of Vacuum Science and Technology A 2006;24 1252-1257. DOI: 10.1116/1.2167081.

[38] Krispin P, Gambin V, Harris JS, Ploog KH. Nitrogen-related electron traps in Ga(As,N) layers (<3%N). Journal of Applied Physics 2003;93 6095-6099. DOI: 10.1063/1.1568523.

[39] Shockley W, Read WT. Statistics of the Recombinations of Holes and Electrons. Physical Review 1952;87 835. DOI: 10.1103/PhysRev.87.835.

[40] Zhang SB, Wei SH. Nitrogen Solubility and Induced Defect Complexes in Epitaxial GaAs:N. Physical Review Letters 2001;86 1789.

[41] Bouzazi B, Lee JH, Suzuki H, Kojima N, Ohshita Y, Yamaguchi M. Origin Investigation of a Nitrogen-Related Recombination Center in GaAsN Grown by Chemical Beam Epitaxy. Japanese Journal of Applied Physics 2011;50 051001.

[42] Saito K, Nishimura K, Suzuki H, Kojima N, Ohshita Y, Yamaguchi M. Hydrogen reduction in GaAsN thin films by flow rate modulated chemical beam epitaxy. Thin Solid Films 2008;516 3517-3520. DOI: 10.1016/j.tsf.2007.08.022.

[43] Janotti A, Wei SH, Zhang SB, S. Kurtz, Van de Walle CG. Interactions between nitrogen, hydrogen, and gallium vacancies in $GaAs_{1-x}N_x$ alloys. Physical Review B 2003;67 161201. DOI: 10.1103/PhysRevB.67.161201.

[44] Toivonen J, Hakkarainen T, Sopanen M, Lipsanen H, Oila J, Saarinen K. Observation of defect complexes containing Ga vacancies in GaAsN. Applied Physics Letters 2003;82 40-42. DOI: 10.1063/1.1533843.